Inorg. Chem. **2007**, *46*, 552–560

Mixed Co–Rh Nitrido-Encapsulated Carbonyl Clusters. Synthesis, Solid-State Structure, and Electrochemical/EPR Characterization of the Anions $[Co_{10}Rh(N)_2(CO)_{21}]^{3-}$, $[Co_{10}Rh_2(N)_2(CO)_{24}]^{2-}$, and $[Co_{11}Rh(N)_2(CO)_{24}]^{2-}$

Michela Costa,[†] Roberto Della Pergola,[‡] Alessandro Fumagalli,*[,†] Franco Laschi,[#] Serena Losi,[#] Piero Macchi,[§] Angelo Sironi,*[,§] and Piero Zanello*[,#]

Dipartimento di Biologia Strutturale e Funzionale dell'Università degli Studi dell'Insubria, Via J. H. Dunant 3, 21100 Varese, Italy, Dipartimento di Scienze dell'Ambiente e del Territorio dell'Università di Milano-Bicocca, Piazza della Scienza 1, 20126 Milano, Italy, Dipartimento di Chimica Strutturale e Stereochimica Inorganica dell'Università di Milano, Via G. Venezian 21, 20133 Milano, Italy, Dipartimento di Chimica dell'Università di Siena, Via Aldo Moro, 53100 Siena, Italy

Received May 15, 2006

The nitrido-encapsulated heterometallic cluster anions $[Co_{10}Rh(N)_2(CO)_{21}]^{3-}$ (**1**), $[Co_{10}Rh_2(N)_2(CO)_{24}]^{2-}$ (**2**), and $[Co_{11}Rh(N)_2(CO)_{24}]^{2-}$ (**3**) have been obtained by tailored redox-condensation reactions. These three anions are rare high-nuclearity mixed-metal clusters containing two interstitial nitrogen atoms. Their structures have been determined by single-crystal X-ray diffraction on their $[NR_4]^+$ salts (R = Me for **1** and **3**, R = Et for **2**), and their electrochemical and ESR properties have been studied in detail. It is noteworthy that **1** has an unprecedented stereochemistry that does not exhibit a close geometrical resemblance with the isoelectronic homometallic anion $[Co_{11}N_2(CO)_{11}(\mu_2\text{-}CO)_{10}]^{3-}$, and **2**, despite its even number of electrons, is a paramagnetic species.

Introduction

Interstitial main group atoms (C, N, P, etc.) play an essential role in the build up of high-nuclearity metal carbonyl clusters. Unlike conventional ligands, they can contribute to the number of cluster valence electrons with no steric requirements on the cluster surface. In particular, encapsulated nitrido species are quite appealing not only because nitrogen atoms may donate up to five electrons but also because they show a distinctive aptitude toward unusual stereochemistries and coordination numbers within the interstitial cavity, which give rise to singular cluster shapes.[1] Several homo- and heterometallic carbonyl clusters containing one interstitial nitrogen atom have been synthesized, but so far, quite a few polynitrido species have been reported; these are mostly cobalt or rhodium clusters and have been generally derived from the prototypical N-encapsulated trigonal prismatic anions $[Co_6N(CO)_{15}]^-$,[2] and $[Rh_6N(CO)_{15}]^-$,[3] respectively. Namely, these high-nuclearity anions containing two, three, or four nitrogen atoms, are $[Co_{10}(N)_2(CO)_{19}]^{4-}$,[4] $[Co_{11}(N)_2(CO)_{21}]^{3-}$,[5] $[Co_{13}(N)_2(CO)_{24}]^{3-}$,[6] $[Co_{14}(N)_3(CO)_{26}]^{3-}$,[7] $[Rh_{12}(N)_2(CO)_{23}H]^{3-}$,[8] $[Rh_{14}(N)_2(CO)_{25}]^{2-}$,[9] $[Rh_{23}(N)_4(CO)_{38}]^{3-}$,[10]

* To whom correspondence should be addressed. E-mail: alessandro.fumagalli@uninsubria.it (A.F., synthesis); angelo.sironi@istm.cnr.it (A.S., structural considerations); zanello@unisi.it (P.Z., electrochemistry and EPR). Phone: +39 0332 421548 (A.F.). Fax: +39 0332 421554 (A.F.).

[†] Università dell'Insubria.

[‡] Università di Milano-Bicocca.

[§] Università di Milano.

[#] Università di Siena.

(1) Fumagalli, A.; Della Pergola, R. *Metal Clusters in Chemistry*; Braunstein P., Oro, L. A., Raithby, P. R., Eds.; Wiley-VCH: Weinheim, Germany, 1999; Vol. 1, 323−347.

(2) Martinengo, S.; Ciani, G.; Sironi, A.; Heaton, B. T.; Mason, J. *J. Am. Chem. Soc.* **1979**, *101*, 7095.

(3) Bonfichi, R.; Ciani, G.; Sironi, A.; Martinengo, S. *J. Chem. Soc., Dalton Trans.* **1983**, 253.

(4) Fumagalli, A.; Martinengo, S.; Tasselli, M.; Ciani, G.; Macchi, P.; Sironi, A. *Inorg. Chem.* **1998**, *37*, 2826.

(5) Fumagalli, A.; Ulivieri, P.; Costa, M.; Crispu, O.; Della Pergola, R.; Fabrizi de Biani, F.; Laschi, F.; Zanello, P.; Macchi, P.; Sironi, A. *Inorg. Chem.* **2004**, *43*, 2125−2131.

(6) Fumagalli, A.; Costa, M.; Della Pergola, R.; Zanello, P.; Fabrizi de Biani, F.; Macchi, P.; Sironi, A. *Inorg. Chim. Acta* **2003**, *350*, 187−192.

(7) Martinengo, S.; Ciani, G.; Sironi, A. *J. Organomet. Chem.* **1988**, *358*, C23.

(8) Martinengo, S.; Ciani, G.; Sironi, A. *J. Chem. Soc., Chem. Commun.* **1986**, 1742.

10.1021/ic0608288 CCC: $37.00
Published on Web 12/22/2006

and $[Rh_{28}(N)_4(CO)_{41}H_x]^{4-}$.[11] Quite recently we have also reported the first examples of dinitrido mixed-metal clusters, the anions $[Fe_6Ni_6(N)_2(CO)_{24}]^{n-}$ ($n = 2, 3, 4$).[12]

In this paper we report on three new high-nuclearity mixed-metal dinitrido clusters, one eleven-metal trianion, and two twelve-metal dianions that have been obtained by tailored redox-condensation reactions. It has been demonstrated, both experimentally and theoretically, that substitution of one metal by another in isostructural compounds can modify the physicochemical properties of the compounds, in particular, their redox reactivity[13] and magnetic behavior.[14] Furthermore, this work shows that the substitution of cobalt with rhodium can result in either of the isostructural anions $[Co_{10}Rh_2(N)_2(CO)_{24}]^{2-}$ (**2**) and $[Co_{11}Rh(N)_2(CO)_{24}]^{2-}$ (**3**) or in species that are geometrically different, as is the case of $[Co_{11}(N)_2(CO)_{21}]^{3-}$ and $[Co_{10}Rh(N)_2(CO)_{21}]^{3-}$ (**1**).

An ESR examination of $[Co_{10}Rh_2(N)_2(CO)_{24}]^{2-}$ (**2**) and structural analogies with the previously quoted Fe−Ni−N anions suggest that the trioctahedral clusters may be genuine examples of paramagnetic behavior in carbonyl complexes.[15] However, since this question was extensively examined some years ago, with inconclusive results,[16] we plan to undertake an additional investigation, including more quantitative measurements of their spin moments.

Results and Discussion

1. Synthesis of 11- and 12-Metal Mixed Cluster. The high anionic charge makes $[Co_{10}(N)_2(CO)_{19}]^{4-}$ quite reactive toward electrophilic reagents. Because of this, we tried an expansion of the metallic cage by means of redox-condensations[17] with Rh(I) mononuclear fragments. Both $[Rh(CO)_2(MeCN)_2]^+$ (as a BF_4^- salt) and $[Rh(CO)_2Cl]_2$ instantaneously react with the tetraanion (as the $[Cs]^+$ salt in MeCN). IR monitoring of these reactions show, at first, a product with a characteristic IR spectrum (1961s, 1805 m). However, this is only an intermediate product which, within minutes, evolves toward the stable anion **1**. The two Rh(I) precursors react with different stoichiometries. The reaction of the cationic Rh(I) species involves a simple "net" addition of the $Rh(CO)_2^+$ fragment

$$[Co_{10}(N)_2(CO)_{19}]^{4-} + [Rh(CO)_2(MeCN)_2]^+ \rightarrow [Co_{10}Rh(N)_2(CO)_{21}]^{3-}\ (\mathbf{1}) + 2MeCN \quad (1)$$

The neutral dimeric species $[Rh(CO)_2Cl]_2$ reacts according to eq 2, with an amount of Rh(I) twice that in the previous reaction, because of the side formation of the square-planar anionic species $[Rh(CO)_2Cl_2]^-$ which is unreactive with respect to the condensation

$$[Co_{10}(N)_2(CO)_{19}]^{4-} + [Rh(CO)_2Cl]_2 \rightarrow [Co_{10}Rh(N)_2(CO)_{21}]^{3-} + [Rh(CO)_2Cl_2]^- \quad (2)$$

Anion **1** undergoes further addition of Rh(I), yielding the 12-metal cluster anion **2**

$$[Co_{10}Rh(N)_2(CO)_{21}]^{3-} + [Rh(CO)_2(MeCN)_2]^+ \rightarrow [Co_{10}Rh_2(N)_2(CO)_{24}]^{2-}\ (\mathbf{2}) + 2\ MeCN \quad (3)$$

It should be noted that eq 3 is one CO short of the 24 required in the balance, and yet the reaction runs with fairly good yields (65%), probably because of the partial decomposition which makes some CO available. A reaction with an excess of Rh(I) does not result in further condensation.

Both anions **1** and **2** can be easily recovered by cation metathesis, generally with $[NMe_4]^+$, and are fairly stable so that recrystallization was effective in obtaining crystalline samples suitable for the reported X-ray structural determinations.

These results suggested a possible synthesis of a 12-metal cluster with a different Rh content. The parent compound was the $[Co_{11}(N)_2(CO)_{21}]^{3-}$ trianion that successfully produced the anion **3**, with a stoichiometry analogous to the previous one

$$[Co_{11}N_2(CO)_{21}]^{3-} + [Rh(CO)_2(MeCN)_2]^+ \rightarrow [Co_{11}RhN_2(CO)_{24}]^{2-}\ (\mathbf{3}) + 2MeCN \quad (4)$$

In this case, reaction with an excess of $[Rh(CO)_2(MeCN)_2]^+$ (up to 5 times) did not result in further condensations of **3**.

2. Electrochemistry and Joint EPR Measurements. The dianions $[Co_{10}Rh_2(N)_2(CO)_{24}]^{2-}$ (**2**) and $[Co_{11}Rh(N)_2(CO)_{24}]^{2-}$ (**3**) are electrochemically indistinguishable in that they afford virtually identical cyclic voltammetric (CV) profiles. Figure 1 shows a typical voltammetric response exhibited by **2** in MeCN solution. Three sequential reductions and one oxidation are observed, all exhibiting more or less pronounced features of chemical reversibility. Controlled potential coulometry ascertained that the two first reductions involve one-electron processes per cluster. Cyclic and hydrodynamic voltammetric tests[18] on solutions resulting from step-by-step

(9) Martinengo, S.; Ciani, G.; Sironi A. *J. Chem. Soc., Chem. Commun.* **1991**, 26.
(10) Martinengo, S.; Ciani, G.; Sironi A. *J. Chem. Soc., Chem. Commun.* **1992**, 1405.
(11) Fumagalli, A.; Martinengo, S.; Bernasconi, G.; Ciani, G.; Proserpio, D. M.; Sironi, A. *J. Am. Chem. Soc.* **1997**, *119*, 1450 and references therein.
(12) Della Pergola, R.; Bruschi, M.; Fabrizi de Biani, F.; Fumagalli, A.; Garlaschelli, L.; Laschi, F.; Manassero, M.; Sansoni, M.; Zanello, P. *C. R. Chim.* **2005**, *8*, 1850−1855.
(13) Femoni, C.; Iapalucci, M. C.; Longoni, G.; Svensson, P. H.; Zanello, P.; Fabrizi de Biani, F. *Chem. Eur. J.* **2004**, *10*, 2318
(14) Pacchioni, G.; Rosch, N. *Acc. Chem. Res.* **1995**, *28*, 390
(15) Riccò, M.; Shiroka, T.; Carretta, S.; Bolzoni, F.; Femoni, C.; Iapalucci, M. C.; Longoni, G. *Chem. Eur. J.* **2005**, *11*, 2856
(16) (a) Benfield, R. E.; Edwards, P. P.; Stacy, A. M. *J. Chem. Soc., Chem. Commun.* **1982**, 525. (b) Johnson, D. C.; Benfield, R. E.; Edwards, P. P.; Nelson, W. H. J.; Vargas, M. D. *Nature* **1985**, *314*, 231. (c) Teo, B. K.; Salvo, F. J. D.; Waszczak, J. W.; Longoni, G.; Ceriotti, A. *Inorg. Chem.* **1986**, *25*, 2262. (d) Pronk, B. J.; Brom, H. B.; De Jongh, L. J.; Longoni, G.; Ceriotti, A. *Solid State Commun.* **1986**, *59*, 349. (e) Drake, S. R.; Edwards, P. P.; Johnson, B. F. G.; Lewis, J.; Marseglia, E. A.; Obertelli, S. D.; Pyper, N. C. *Chem. Phys. Lett.* **1987**, *139*, 336. (f) DeAguiar, J. A. O.; Mees, A.; Darriet, J.; De Jongh, L. J.; Drake, S. R.; Edwards, P. P.; Johnson, B. F. G. *Solid State Commun.* **1988**, *66*, 913. (g) Benfield, R. E. *Z. Phys. D* **1989**, *12*, 453.
(17) A definition of redox condensations as "reactions between coordinatively saturated species in different oxidation state" was given by Chini, P.; Longoni, G.; Albano, V. G. *Adv. Organomet. Chem.* **1976**, *14*, 313.
(18) Zanello, P. *Inorganic Electrochemistry. Theory, Practice and Application*; Royal Society of Chemistry: Cambridge, U.K., 2003.

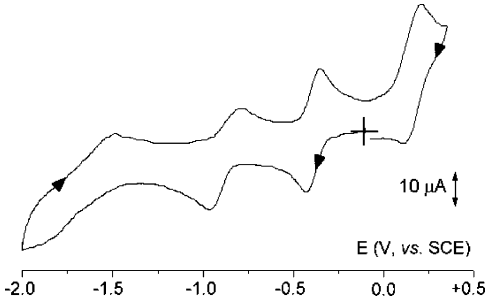

Figure 1. Cyclic voltammetric response recorded at a platinum electrode in a MeCN solution of the $[Co_{10}Rh_2(N)_2(CO)_{24}]^{2-}$ dianion (**2**) (1.2×10^{-3} mol dm^{-3}) with $[NBu_4][PF_6]$ (0.2 mol dm^{-3}) supporting electrolyte and a scan rate of 0.2 V s^{-1}.

Table 1. Formal Electrode Potentials (V vs SCE) and Peak-to-Peak Separations (mV) for the Redox Processes Exhibited by $[Co_{10}Rh(N)_2(CO)_{21}]^{3-}$ (**1**), $[Co_{10}Rh_2(N)_2(CO)_{24}]^{2-}$ (**2**), and $[Fe_6Ni_6(N)_2(CO)_{24}]^{2-}$ (**4**) in MeCN Solution

	$E^{\circ\prime}$ (ox)[a]	ΔE_p[b]	i_{pc}/i_{pa}[b]	$E^{\circ\prime}$ (1st red)[c]	ΔE_p[d]	i_{pc}/i_{pa}[d]	$E^{\circ\prime}$ (2nd red)[c]	ΔE_p[d]	i_{pc}/i_{pa}[d]
1	−0.24	79	0.3	−1.07	120	1.0			
2	+0.16	77	0.5	−0.39	106	1.0	−0.88	110	1.0
4	+0.17	74	0.7	−0.40	66	1.0	−0.90	62	1.0

[a] Two-electron oxidation. [b] Measured at 1.0 V s^{-1}. [c] One-electron reduction. [d] Measured at 0.2 V s^{-1}.

exhaustive electrolysis are in accordance with the complete chemical reversibility of these one-electron reductions. In contrast, from a qualitative viewpoint, the most cathodic step ($E^{\circ\prime} \approx -1.7$ V) appears to be accompanied by chemical complications or to be the result of two partially overlapping electron-transfer processes, with only the first one possessing features of partial chemical reversibility.

The anodic process should involve an electrode mechanism consisting of a catalytic regeneration of the reagent (namely, at low scan rates the CV profile assumes a sigmoidal shape, whereas the current function, $i_{pa}/v^{1/2}$, significantly increases upon a decrease of the scan rate). Nevertheless, because it is difficult to justify the presence of a strong reducing agent, we suggest that the oxidation process involves an ECE mechanism in which two electron transfers occur at the same potential value.[18] In fact, such redox activity is qualitatively reminiscent with that of the isoelectronic and isostructural dianion $[Fe_6Ni_6(N)_2(CO)_{24}]^{2-}$ (**4**), in which a two-electron oxidation was detected.[12]

The formal electrode potentials of the above-discussed electron-transfer processes of **2** are compiled in Table 1, together with those of $[Co_{10}Rh(N)_2(CO)_{21}]^{3-}$ (**1**) which will be discussed below.

In view of its stability, EPR measurements were carried out on the electrogenerated anion $[\mathbf{2}]^-$, namely, $[Co_{10}Rh_2N_2(CO)_{24}]^{3-}$. Figure 2 displays the pertinent X-band EPR spectra in glassy CH_3CN solutions.

The line-shape analysis is suitably performed taking into account the main $S = {}^1/_2$ electron-spin Hamiltonian.[19,20] The

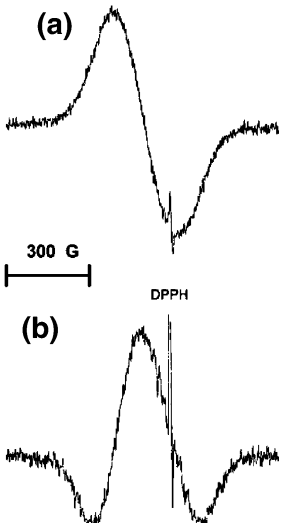

Figure 2. X-band EPR spectra of $[\mathbf{2}]^-$ ($[Co_{10}Rh_2(N)_2(CO)_{24}]^{3-}$) in CH_3CN solution: (a) first-derivative mode and (b) second-derivative mode. $T = 105$ K.

computed[21] g_{av} value of 2.068(8) ($a_{av} = 20(8)$ G) significantly differs from that of the free electron, $g_{electron} = 2.0023$. The large ΔH_{av} value of 210(8) G accounts for the broad and unresolved pseudoisotropic absorption (first-derivative mode).

In agreement with the DFT calculations on the isostructural anion $[Fe_6Ni_6(N)_2(CO)_{24}]^{3-}$,[12] the paramagnetic features, which are typical of the metallic character enhanced by the Co and Rh spin−orbit interactions, point to the marked delocalization of the unpaired spin density present in the metal-centered SOMO. The second-derivative spectrum reveals the presence of a series of narrow signals centered within the intermediate region of the broad absorption, Figure 2b. Such a pattern supports the direct hyperfine interaction of the $S = {}^1/_2$ electron with different magnetically active nuclei of the metal skeleton. In fact, two cobalt nuclei could be involved in the direct magnetic coupling with the $S = {}^1/_2$ unpaired electron or conversely one cobalt and one or two rhodium nuclei. As an alternative picture, the multiplet could also arise from the magnetic contribution of the two encapsulated nitrogen atoms ^{14}N ($I = 1$, natural abundance = 99.6%) to the overall glassy line-shape in the presence of magnetic nonequivalence, theoretically producing one triplet of triplets.

The poor hpf resolution of the glassy spectrum is not surprising in the presence of the high-nuclearity of the paramagnetic cluster.[19,20]

When the temperature is increased to the glassy-fluid transition phase ($T = 226$ K), the anisotropic spectrum disappears, and the fluid solution becomes EPR silent in that the active intramolecular dynamics under fast-motion conditions trigger effective electron-spin relaxation processes.[19,20]

Rapid refreezing of the fluid solution quantitatively regenerates the previous broad line-shape, indicating the stability of the anion.

(19) Mabbs, F. E.; Collison, D. *Electron Paramagnetic Resonance of d Transition Metal Compounds*; Studies in Inorganic Chemistry, Vol. 16; Elsevier: New York, 1992.
(20) Drago, R. S. *Physical Methods for Chemists*; Saunders College: New York, 1992.
(21) Lozos, G. P.; Hoffman, B.; Franz, C. G. *SIM14/SIM14A: Simulation of Powder EPR Spectra*; Northwestern University, Evanston, Illinois, 1974; *Quantum Chemistry Program Exchange*, **1974**, *11*, 265.

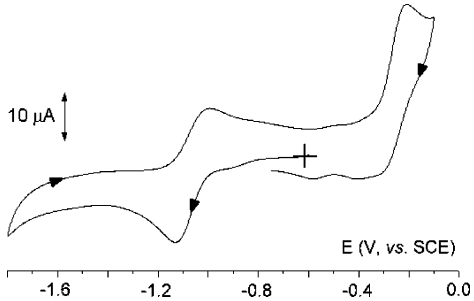

Figure 3. Cyclic voltammetric response recorded at a platinum electrode in a MeCN solution of $[Co_{10}Rh(N)_2(CO)_{21}]^{3-}$ **(1)** (1.4×10^{-3} mol dm^{-3}) with $[NBu_4][PF_6]$ (0.2 mol dm^{-3}) supporting electrolyte and a scan rate of 0.2 V s^{-1}.

The structural (see below) and electrochemical properties of dianion **2** are similar to those of the $[Fe_6Ni_6(N)_2(CO)_{24}]^{2-}$ dianion.[12] Since theoretical considerations support the $S = 1$ paramagnetic nature of the nitrido-encapsulated Fe−Ni anion, we examined the EPR spectrum of **2**. As a consequence of the active ZFS interactions (ZFS > $h\nu$, ν being the operational frequency), the pertinent EPR parameters significantly differ from those of the corresponding trianion, mainly depending on the electron-spin triplet state.[19,20] In fact, with respect to its trianion $[\mathbf{2}]^-$, the parent dianion **2** exhibits a broad and totally unresolved metal-centered signal ($\Delta H_{av} = 675(10)$ G, $g_{av} = 2.04(6)$) in glassy solution, the experimental line width of which does not allow g_i spectral resolution. (Figure S1 in Supporting Information).

In fluid solution, the dianion becomes EPR silent, likely, because of the temperature-induced fastening of the electron-spin relaxation processes.[19] In agreement, the rapid refreezing of the solution quantitatively restores the glassy spectrum, thus testifying for the chemical stability of the dianion under different experimental conditions.

A different CV pattern is exhibited by $[Co_{10}Rh(N)_2(CO)_{21}]^{3-}$ (**1**). As illustrated in Figure 3, it displays either a single one-electron reduction ($E^{\circ\prime} = -1.06$ V) or an apparent two-electron oxidation ($E^{\circ\prime} = -0.24$ V) in MeCN solution; both are complicated by the accompanying chemical reactions.

In fact, the reduction process appears to involve slow chemical complications in that the i_{pa}/i_{pc} ratio is 0.85 at 0.02 V s^{-1} and reaches the unity value at 0.1 Vs^{-1}. In contrast, the oxidation process is complicated by fast chemical reactions in that the directly associated reduction peak appears only at high scan rates (>1.0 V s^{-1}); for example, at 2.00 V s^{-1}, the i_{pc}/i_{pa} ratio is 0.4. In passing, we note that the presence of very minor unidentified impurities affords barely perceptible peak systems at about −0.5 and −0.9 V.

The formal electrode potentials of the redox changes exhibited by **1** are summarized in Table 1.

In confirmation of chemical complications accompanying the **1**/$[\mathbf{1}]^-$ passage (namely, $[Co_{10}Rh(N)_2(CO)_{21}]^{3-}$/$[Co_{10}Rh(N)_2(CO)_{21}]^{4-}$), EPR measurements carried out in frozen solutions upon gradual reduction showed the progressive appearance of two or three broad absorptions that largely overlapped with each other in the intermediate spectral region (total glassy line width = 410(8) G). The relative g_{av} values ranged from 2.030(8) to 2.095(8), typical of metallic fragments.

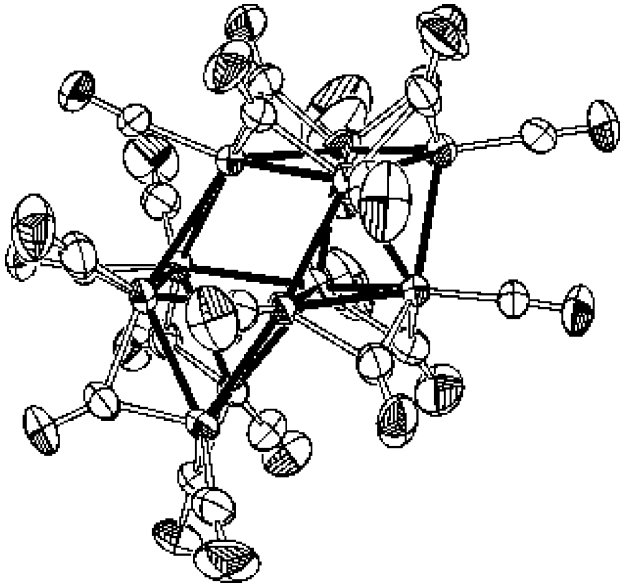

Figure 4. View of the ligand stereochemistry of the $[Co_{10}RhN_2(CO)_{21}]^{3-}$ trianion, **1**.

When the temperature is increased at the glassy-fluid transition, the anisotropic signals disappear, and the fluid solution becomes EPR silent.

3. Crystal Structures of Anions 1, 2, and 3. The overall stereochemistry and a selection of pertinent bond distances of the $[Co_{10}Rh(N)_2(CO)_{11}(\mu_2\text{-}CO)_{10}]^{3-}$ anion (**1**) are presented in Figure 4 and Table 2, respectively.

Anion **1** possesses an asymmetric (C_1) metal framework composed of two capped trigonal prisms (each containing an interstitial nitrido atom) that share a triangular face (see Figure 5a). This cluster does not show a simple geometrical relationship with either the isoelectronic homometallic $[Co_{11}N_2(CO)_{11}(\mu_2\text{-}CO)_{10}]^{3-}$ anion (which possesses a "bent", C_{2v} symmetric, bi-octahedral metal cage containing two interstitial N atoms, one for each octahedral cavity, 3.28 Å apart) or $[Co_{11}(C_2)(CO)_{11}(\mu_2\text{-}CO)_{11}]^{3-}$ (which has a tricapped cubic metal cage of C_s symmetry, with a large internal cavity containing a C_2 unit (C−C 1.62(5) Å)).[22]

The eleven metal vertexes of the $Co_{10}Rh$ core in **1** have different M−M connectivities, being 4 three-, 4 four-, and 3 hexa-connected. As expected, the rhodium atom occupies one of the hexa-connected sites. Although the three hexa-connected metal sites (all belonging to the shared, central Rh−Co1−Co2 triangle) are equally available to the Rh atom, no structural disorder is observed. Hence, it is reasonable to propose that $[Co_{10}Rh(N)_2(CO)_{21}]^{3-}$ is obtained from its parent $[Co_{10}(N)_2(CO)_9(\mu_2\text{-}CO)_{10}]^{4-}$ anion when a $[Rh(CO)_2]^+$ moiety, upon capping the square face of the central prismatic unit (as outlined in Figure 5c), promotes a slight reorganization of the upper prismatic cage to achieve higher M−M connectivity.

Since the $[Co_{10}Rh(N)_2(CO)_{21}]^{3-}$ metal cage consists of two capped trigonal prisms sharing a triangular face, we may use Mingos' condensed polyhedron rule[23] to derive its

(22) Albano, V. G.; Braga, D.; Ciani, G.; Martinengo, S. *J. Organomet. Chem.* **1981**, *213*, 293.
(23) Mingos, D. M. P. *J. Chem. Soc., Chem. Commun.* **1983**, 706.

Table 2. Selected Bond Distances (in Å) for $[Co_{10}Rh(N)_2(CO)_{21}]^{3-}$ (**1**)

Rh−Co(1)	2.924(2)	Co(2)−Co(3)	2.431(2)
Rh−Co(2)	3.093(2)	Co(2)−Co(5)	2.569(2)
Rh−Co(4)	2.666(2)	Co(2)−Co(8)	2.565(2)
Rh−Co(5)	2.653(2)	Co(4)−Co(3)	2.627(2)
Rh−Co(9)	2.860(2)	Co(4)−Co(6)	2.466(2)
Rh−Co(10)	2.842(2)	Co(6)−Co(3)	2.511(2)
Co(1)−Co(3)	2.441(2)	Co(6)−Co(5)	2.446(2)
Co(1)−Co(2)	2.565(2)	Co(7)−Co(8)	2.433(2)
Co(1)−Co(4)	2.530(2)	Co(7)−Co(9)	2.502(2)
Co(1)−Co(7)	2.615(2)	Co(10)−Co(9)	2.480(2)
Co(1)−Co(9)	2.491(2)	Co(10)−Co(8)	2.513(2)
		Co(10)−Co(2)	2.621(2)
Rh−N(1)	2.182(7)	Co(1)−N(2)	1.936(7)
Co(1)−N(1)	2.424(7)	Co(2)−N(2)	1.951(7)
Co(2)−N(1)	2.000(7)	Co(7)−N(2)	1.902(7)
Co(3)−N(1)	1.978(7)	Co(8)−N(2)	1.915(8)
Co(4)−N(1)	1.905(8)	Co(9)−N(2)	1.935(7)
Co(5)−N(1)	1.903(7)	Co(10)−N(2)	1.938(7)
Co(6)−N(1)	1.923(7)		
Rh−C(0)	1.83(1)	Co(1)−C(1)	1.69(1)
Co(2)−C(2)	1.74(2)	Co(3)−C(3)	1.73(1)
Co(4)−C(4)	1.72(1)	Co(5)−C(5)	1.71(2)
Co(6)−C(6)	1.73(1)	Co(7)−C(7)	1.73(1)
Co(8)−C(8)	1.75(1)	Co(9)−C(9)	1.75(1)
Co(10)−C(10)	1.73(1)		
Rh−C(40)	2.09(1)	Co(4)−C(40)	1.86(1)
Rh−C(50)	2.01(1)	Co(5)−C(50)	1.89(1)
Co(1)−C(13)	1.89(1)	Co(3)−C(13)	1.86(1)
Co(2)−C(23)	1.99(1)	Co(3)−C(23)	1.81(1)
Co(4)−C(46)	1.92(1)	Co(6)−C(46)	1.86(1)
Co(5)−C(56)	1.89(1)	Co(6)−C(56)	1.85(1)
Co(7)−C(78)	1.88(1)	Co(8)−C(78)	1.91(1)
Co(7)−C(79)	1.87(1)	Co(9)−C(79)	1.96(1)
Co(8)−C(810)	1.90(1)	Co(10)−C(810)	1.91(1)
Co(9)−C(910)	1.92(1)	Co(10)−C(910)	1.90(1)
<> C−O term	1.14	<> C−O bridg	1.17

expected cluster valence electron (CVE) number. Thus, for a prism condensed with a square pyramid through a square face, we expect (90 + 74 − 64) 100 CVEs, as observed for $[Rh_6MN(CO)_{15}]^{2-}$ (M = Co, Rh, Ir),[24] while upon a self-condensation through a triangular face, we expect (100 + 100 − 48) 152 CVEs. Actually, the $[Co_{10}RhN_2(CO)_{21}]^{3-}$ anion possesses two more CVEs (i.e., 154), and we have to look at its stereochemistry in more detail to ascertain the origin of this discrepancy.[25] Consistent with the low symmetry of the cluster, the metal−metal bond distances are rather wide. As usual, the unbridged Co−Co interactions (nine, range of 2.491−2.627 Å, av 2.575 Å) are, on average, longer than the bridged ones (eight, range of 2.431−2.513 Å, av 2.467 Å), but there is a slight overlap of the ranges. As far as the six Co−Rh interaction are concerned, the four unbridged ones average 2.930 Å, while the two bridged ones average 2.660 Å. However, two of the four unbridged Rh−Co bonds (dashed in Figure 5b) are clearly longer than the other two probably because the two excess electrons are localized there.

As far as the interstitial nitrides are concerned, it is remarkable is that the two nitride environments are different: N(2) resides in a regular trigonal prismatic cage displaying similar Co−N(2) interactions (six, range of 1.902−1.951 Å, av 1.930 Å); in contrast, N(1) is located within a capped trigonal prism in a very asymmetric environment. This is related both to the presence of the unique rhodium atom in one of the vertices of the prism (Rh−N(1) = 2.182 Å vs Co(2−6)−N(1) range = 1.903−2.000 Å, av 1.942 Å) and to the presence of a long interaction with the capping atom (Co(1)−N(1) = 2.424 Å).

The two isoelectronic dianions, $[Co_{10}Rh_2(N)_2(CO)_{12}(\mu_2\text{-}CO)_{12}]^{2-}$ (**2**) and $[Co_{11}Rh(N)_2(CO)_{12}(\mu_2\text{-}CO)_{12}]^{2-}$ (**3**), possess the very same metal core (a face-sharing trioctahedron) and have analogous ligand stereochemistry (see Figure 6a) with similar bonding parameters (see Table 3).

As shown in Figure 7, the geometry of the metal framework consists of a hexagonal close-packed fragment derived from the *abab* stacking of four triangles. The resulting trioctahedron possesses pseudo-D_{3d} symmetry. Note that the Rh atoms are randomly disordered over the six metal atoms of the central octahedron, thus confirming the preference of the heavier atoms for the sites having the larger metal−metal connectivities. The ligand stereochemistry is quite "regular", all of the metals being connected to one terminal and two bridging carbonyls. The latter (semi-)bridging COs occupy the interbasal edges of the two external octahedra; the M(1,2,3)−C bond lengths (2.21 Å av) are systematically longer than the Co(4,5,6)−C ones (1.85 Å av). Both **2** and **3** lie on crystallographic centers of symmetry, but the symmetric disposition of the ligands and the Rh crystal disorder allow a much higher pseudosymmetry (D_{3d}).

The stereochemistry of **2** and **3** is related to that of the known octahedral $[Co_6N(CO)_{13}]^-$ monoanion[26] (Figure 6b) and, apart from the presence of the Rh atoms, can be thought to be obtained by the coupling of two such cluster anions (along with the loss of two carbonyls). $[Co_{10}Rh_2(N)_2(CO)_{24}]^{2-}$ (and **3**) is isoelectronic and somewhat similar to the $[Fe_6Ni_6(N)_2(CO)_{24}]^{2-}$ anion,[12] the major geometrical difference being the lack of bridging carbonyls in the latter species (this is related to the different electronic requirements of Ni and Fe atoms).

The stacking of four metal triangles has been observed a few times, namely, in $[Pt_{12}(CO)_{12}(\mu_2\text{-}CO)_{12}]^{2-}$ (triprismatic metal framework, 170 CVEs),[27] $[Rh_{12}H_2(CO)_{13}(\mu_2\text{-}CO)_9(\mu_3\text{-}CO)_3]$ (trioctahedral cage, 160 CVEs),[28] $[Ir_{12}(CO)_{18}(\mu_2\text{-}CO)_8]^{2-}$ (trioctahedral cage, 162 CVEs),[29] and the above-mentioned $[Fe_6Ni_6N_2(CO)_{24}]^{n-}$ (n = 2, 3, 4; 168−170 CVEs).[12] According to Mingos' rule, we would expect (3 × 86 − 2 × 48) 162 CVEs for a trioctahedral metal cage, and

(24) Martinengo, S.; Ciani, G.; Sironi, A. *J. Chem. Soc., Chem. Commun.* **1984**, 1577.

(25) The very same result can be obtained by describing the cage as a couple of prisms sharing a vertex which are further interconnected by five bonds (2 × 90 − 1 × 18 − 5 × 2 = 152 CVEs).

(26) The structurally characterized 86-CVE octahedral $[Co_6N(CO)_{13}]^-$ monoanion was prepared by decarbonylation of the 90-CVE trigonal prismatic $[Co_6N(CO)_{15}]^-$ monoanion in THF; under CO, this reaction is reversible. Ciani, G.; Martinengo, S. *J. Organometal. Chem.* **1986**, *306*, C49.

(27) (a) Calabrese, J. C.; Dahl, L. F.; Chini, P.; Longoni, G.; Martinengo S. *J. Am. Chem. Soc.* **1974**, *96*, 2614. (b) Longoni, G.; Chini, P. *J. Am. Chem. Soc.* **1976**, *98*, 7225. (c) Lower, L. D. Ph.D. Thesis, University of Wisconsin, Madison, WI,1976.

(28) Ciani, G.; Sironi, A.; Martinengo, S. *J. Chem. Soc., Chem. Commun.* **1985**, 1757.

(29) Della Pergola, R.; Demartin, F.; Garlaschelli, L.; Manassero, M.; Martinengo, S.; Sansoni, M. *Inorg. Chem.* **1987**, *26*, 3487.

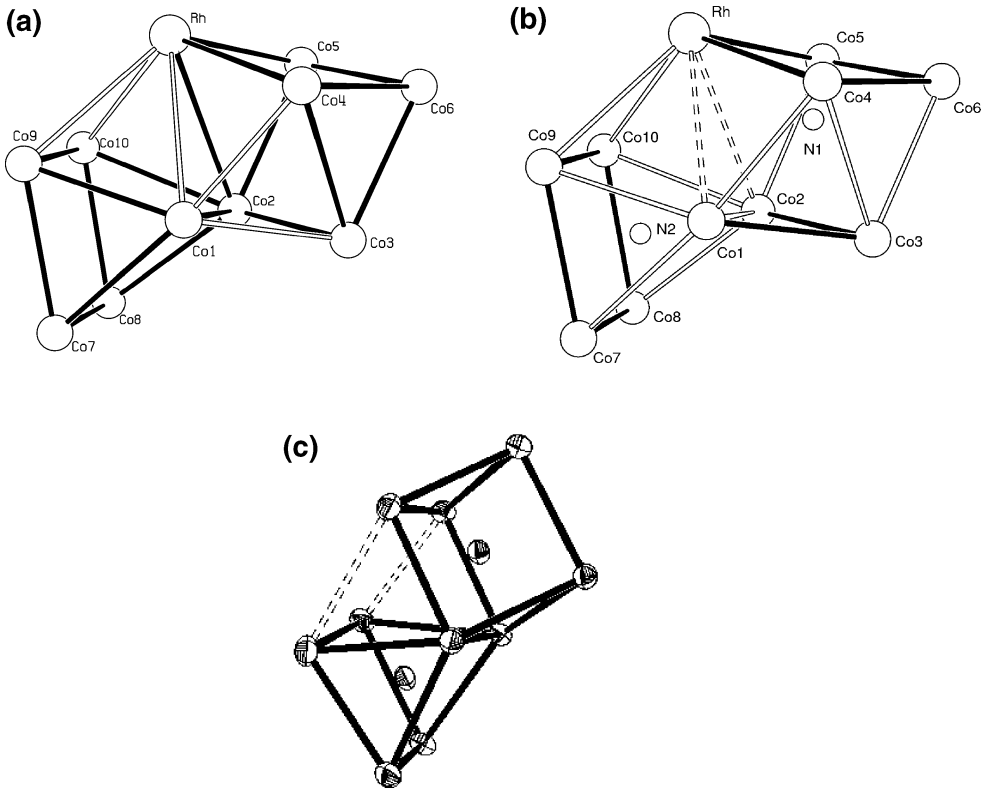

Figure 5. Different views of the metal cage present in the $[Co_{10}RhN_2(CO)_{21}]^{3-}$ anion, highlighting (a) the build up of the cluster from two capped trigonal prisms sharing a triangular face and (b) the distribution of bridging carbonyls (which insists on the filled edges) and the two lengthened Rh−Co bonds. (c) $[Co_{10}RhN_2(CO)_{21}]^{3-}$ can also be formally obtained by capping the square face of the central prismatic unit of the parent $[Co_{10}N_2(CO)_{19}]^{4-}$ anion (and reorganizing some M−M bonds).

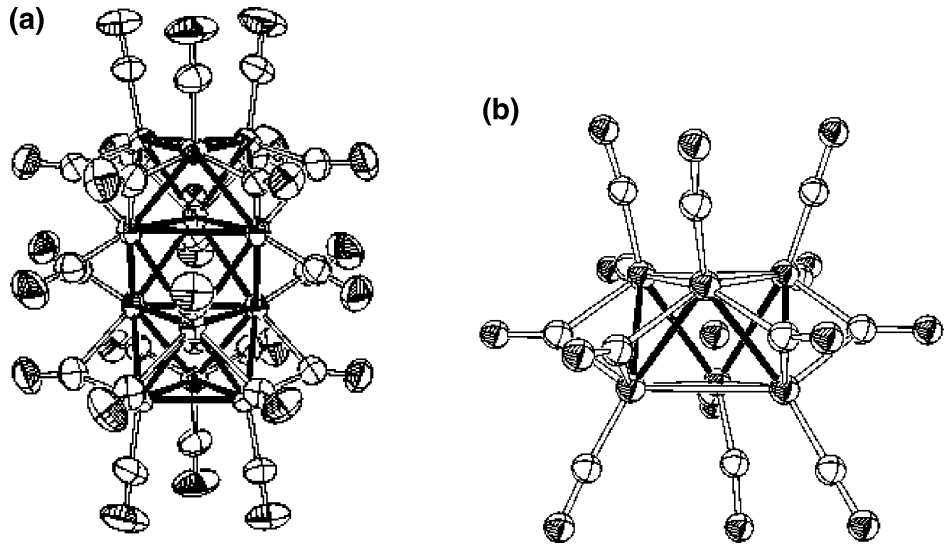

Figure 6. (a) View of the $[Co_{10}Rh_2(N)_2(CO)_{24}]^{2-}$ dianion (**2**) of pseudo-D_{3d} symmetry. Its geometry is analogous to that of the $[Co_{11}Rh(N)_2(CO)_{24}]^{2-}$ dianion (**3**). (b) View of the known octahedral $[Co_6N(CO)_{13}]^-$ monoanion of pseudo-C_s symmetry.

yet both **2** and **3** possess 168 CVEs. Again, this anomalous electron bookkeeping is presumably related to some polyhedral distortion. Actually, cobalt octahedral cavities are not well suited for hosting an interstitial first-row element, and large polyhedral distortions are normally observed. For instance, the Co−Co bond distances in the octahedral $[Co_6N(CO)_{13}]^-$ anion[30] span the 2.487−2.788 Å range (av 2.502 and 2.669 Å for the four CO-bridged and the ten unbridged Co−Co edges, respectively), while in the $[Co_6C(CO)_{13}]^{2-}$ anion,[31] they span the 2.465−2.926 Å range (av 2.483 and 2.750 Å for the five CO-bridged and the nine unbridged Co−Co edges, respectively). Both clusters have the expected number of CVEs (86).[32] In **2**, the metal−metal

(30) Martinengo, S.; Ciani, G. *J. Organomet. Chem.* **1986**, *306*, C49.

(31) Albano, V. G.; Braga, D.; Martinengo, S. J. *Chem. Soc., Dalton Trans.* **1986**, 981.

(32) Actually, the related $[Co_6C(CO)_{14}]^-$ anion has 87 CVEs. Albano, V. G.; Ciani, G.; Sansoni, M.; Martinengo, S. *J. Chem. Soc., Dalton Trans.* **1980**, 163.

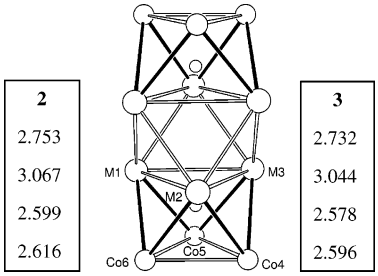

Figure 7. View of the metal framework of the $[Co_{10}Rh_2(N)_2(CO)_{24}]^{2-}$ dianion, **2** (representative also of isostructural $[Co_{11}Rh(N)_2(CO)_{24}]^{2-}$ (**3**)), highlighting the labeling of the symmetry independent part (i.e., each cluster has a crystallographic inversion center) and the distribution of bridging carbonyls (which insists on the filled edges). The metal−metal interactions can be grouped into four classes: six basal ones within the two external triangles (av 2.596 and 2.616 Å in **3** and **2**, respectively), six basal ones within the two internal triangles (av 3.044 and 3.067 Å in **3** and **2**, respectively), six interbasal ones within the internal octahedron (av 2.732 and 2.753 Å in **3** and **2**, respectively), and twelve CO-bridged interbasal ones within the two external octahedra (av 2.578 and 2.599 Å in **3** and **2**, respectively).

Table 3. Selected Bond Distances (in Å) for $[Co_{10}Rh_2(N)_2(CO)_{24}]^{2-}$ (**2**) and $[Co_{11}Rh(N)_2(CO)_{24}]^{2-}$ (**3**)

	$[Co_{10}Rh_2N_2(CO)_{24}]^{2-}$	$[Co_{11}RhN_2(CO)_{24}]^{2-}$
M(1)−Co(5)	2.645(1)	2.563(1)
M(1)−Co(6)	2.594(1)	2.564(1)
M(2)−Co(4)	2.552(1	2.581(1)
M(2)−Co(6)	2.544(1)	2.592(1)
M(3)−Co(4)	2.622(1)	2.598(1)
M(3)−Co(5)	2.637(1)	2.568(1)
M(1)−M(2)	3.096(1)	3.048(1)
M(1)−M(3)	2.998(1)	3.044(1)
M(2)−M(3)	3.106(1)	3.038(1)
M(1)−M(3)#1	2.681(1)	2.734(1)
M(1)−M(2)#1	2.781(1)	2.740(1)
M(2)−M(3)#1	2.796(1)	2.721(1)
Co(4)−Co(6)	2.634(1)	2.593(1)
Co(4)−Co(5)	2.603(1)	2.601(1)
Co(5)−Co(6)	2.612(1)	2.593(1)
M(1)−N(1)	1.949(2)	1.911(3)
M(2)−N(1)	1.916(2)	1.918(3)
M(3)−N(1)	1.952(2)	1.917(3)
Co(4)−N(1)	1.913(2)	1.944(3)
Co(5)−N(1)	1.989(2)	1.927(3)
Co(6)−N(1)	1.909(2)	1.934(3)
M(1)−C(1)	1.771(3)	1.740(5)
M(2)−C(2)	1.759(3)	1.747(4)
M(3)−C(3)	1.772(3)	1.741(4)
Co(4)−C(4)	1.748(3)	1.740(5)
Co(5)−C(5)	1.771(3)	1.743(5)
Co(6)−C(6)	1.747(3)	1.753(4)
M(1)−C(15)	2.511(3)	2.191(5)
Co(5)−C(15)	1.807(3)	1.841(5)
M(1)−C(16)	2.094(3)	2.147(4)
Co(6)−C(16)	1.886(3)	1.849(4)
M(2)−C(24)	2.070(3)	2.195(5)
Co(4)−C(24)	1.868(3)	1.842(4)
M(2)−C(26)	2.042(3)	2.249(4)
Co(6)−C(26)	1.865(3)	1.842(4)
M(3)−C(34)	2.145(3)	2.311(5)
Co(4)−C(34)	1.872(3)	1.828(5)
M(3)−C(35)	2.419(4)	2.142(4)
Co(5)−C(35)	1.808(3)	1.862(4)
<> C−O term	1.138	1.140
<> C−O bridg	1.153	1.147

connectivities spread over the 2.544−3.106 Å range (av 2.599 and 2.842 Å for the twelve CO-bridged and twelve unbridged edges of the two external octahedral cages, respectively, while the six remaining interbasal edges of the central octahedron average 2.753 Å).[33] Thus, the six excess CVEs seem to contribute to both (i) an overall expansion of the two octahedral cages hosting the two nitrides (see caption to Figure 7 for the grouping of the M−M interactions into different classes) and (ii) an expansion of the central octahedron for which both intra- and interbasal connectivities are rather long (3.067 and 2.753 Å, respectively). However, we must also consider that part of this geometrical expansion must be accounted for by the presence of two (out of six) Rh atoms disordered over the internal octahedron. In addition, the marked asymmetry of the bridging carbonyls may also contribute to increasing the average of the bridged metal−metal bond distances. In this respect, the stability of the $[\mathbf{2}]^-$ anion (or $[Co_{10}Rh_2(N)_2(CO)_{24}]^{3-}$), established from electrochemical measurement appears to be quite remarkable, considering that a more marked expansion would be expected.

Experimental Section

All operations were carried out under nitrogen with a standard Schlenk tube apparatus. Commercial, anhydrous, inhibitor-free tetrahydrofuran (THF) was used. All other analytical grade solvents were degassed in vacuum and stored under nitrogen with 3 Å molecular sieves. $Cs_4[Co_{10}(N)_2(CO)_{19}]$, $[NMe_4]_4[Co_{10}(N)_2(CO)_{19}]$,[4] $[NMe_4]_3[Co_{11}(N)_2(CO)_{21}]$,[5] and $[Rh(CO)_2(MeCN)_2]BF_4$,[34] were prepared by published methods. Infrared spectra were recorded on Perkin-Elmer 16PC or Nicolet Avatar 360 FT-IR spectrophotometers, using 0.1 mm CaF_2 cells previously purged with nitrogen. Reference IR spectra were obtained with a 20 μL microcell from single crystals (usually selected by the crystallographer when choosing an identical one for the structural determination). Since the C, H, N, analyses are often of little significance,[35] our best criterion to judge the purity is based on the exact fitting of the IR spectrum of an actual sample to the reference one.[36] The products for the CV/ESR measurements were prepared as $[NMe_4]^+$ because of the easy purification. When recovered after a recrystallization process made with the slow diffusion technique, the products were washed thoroughly with *i*-PrOH. This also removed some microcrystalline product, leaving (with considerably lower yields) a little crop of the largest crystals (∼0.1−1 mm). Always, a small sample of it passed the test with reference IR (Table 4).

Materials and apparatus for electrochemistry and EPR measurements have been described elsewhere.[5] Potential values are referred to the saturated calomel electrode (SCE). Under the actual experimental conditions, the one-electron oxidation of ferrocene occurs at $E^{\circ\prime} = +0.38$ V, displaying a peak-to-peak separation of 62 mV at 0.2 V s^{-1}.

1. Synthesis of $[Co_{10}RhN_2(CO)_{21}]^{3-}$ (1) as an $[NMe_4]^+$ Salt. $Cs_4[Co_{10}N_2(CO)_{19}]$ (440 mg, 0.261 mmol) in MeCN (15 mL) was treated at room temperature with $[Rh(CO)_2Cl]_2$ (87 mg, 0.261

(33) The M−M interactions in **3** spread over the 2.563−3.048 Å range (av 2.578 and 2.820 Å for the twelve CO-bridged and twelve unbridged Co-Co edges of the two external octahedral cages, while the six remaining interbasal Co-Co edges of the central octahedron average 2.732 Å).

(34) (a) Ugo, R.; Bonati, F.; Fiore, M. *Inorg. Chim. Acta.* **1968**, *2*, 463. (b) Epstein, R. A.; Geoffrey, G. L.; Keeney, M. E.; Mason, W. R. *Inorg. Chem.* **1979**, *18*, 478.

(35) Generally, C, H, N analyses of interstitial nitrides yield less nitrogen than expected. Fumagalli, A.; Della Pergola R. Unpublished results.

(36) A flat line must result in the IR spectra subtraction, that is, $Abs_{sample} - f \times Abs_{ref}$ (f is an optimized factor). An example of the IR test of purity is reported in Figure S2 of the Supporting Information.

Table 4. IR CO-Stretching Bands (±2 cm^{-1}) of the Anions $[Co_{10}Rh(N)_2(CO)_{21}]^{3-}$ (**1**), $[Co_{10}Rh_2(N)_2(CO)_{24}]^{2-}$ (**2**), and $[Co_{11}Rh(N)_2(CO)_{24}]^{2-}$ (**3**) as $[NMe_4]^+$ Salts

	solvent	terminal COs (cm^{-1})	bridging COs (cm^{-1})
1	MeCN[a]	1978 s, 1968 sh	1813 m
	acetone	2011 w, 1979 s, 1933 w	1819 m
2	MeCN[a]	2016 s, 1998 s	1846 m
			(1713 w, clathrated acetone)
	acetone	2012 s, 2000 s	1847 m
3	MeCN[a]	2015 vs, 1997 s	1842 ms
			(1713 w, clathrated acetone)
	acetone[a]	2011 vs, 1998 s	1851 ms

[a] Single crystal in a 20 μL microcell.

mmol); after it was stirred for 10 min, the solution was evaporated under vacuum. The residue was dissolved in THF and filtered to remove some precipitate. The resulting clear solution was treated dropwise with a solution of $[NMe_4]Cl$ (500 mg) in MeOH (2 mL). After 2 h of stirring, the solution was filtered, and the precipitate was washed with 2-PrOH (3 × 1 mL) and vacuum dried. The product, redissolved in acetone (5 mL), was cautiously layered with 2-propanol (15 mL). When the diffusion was completed (∼1 week), after removal of the decanted mother liquor, the crystalline product was recovered, thoroughly washed with 2-propanol, and vacuum dried. Yield: 187 mg, 47%. The elemental analyses are indicative of a product with no clathrated acetone. Anal. Found (calcd) (%) for $[NMe_4]_3[Co_{10}RhN_2(CO)_{21}]$, $C_{33}H_{36}Co_{10}N_5O_{21}Rh$: C, 25.04 (25.89); H, 2.78 (2.37); N, 3.73 (4.57).[35] The material, sealed under inert atmosphere, maintains its solubility and spectroscopical purity (according to IR, see Table 4).[36]

The redox-condensation may also be performed with $[Rh(CO)_2(MeCN)_2]BF_4$ in a 1:1 molar ratio with $Cs_4[Co_{10}N_2(CO)_{19}]$ using acetone as alternative solvent to MeCN. Subsequent procedures, metathesis, and recrystallization were conducted as described above.

2.a. Synthesis of $[Co_{10}Rh_2N_2(CO)_{24}]^{2-}$ (2) as $[NMe_4]^+$ Salt. $[NMe_4]_4[Co_{10}N_2(CO)_{19}]$ (165 mg, 0.114 mmol) and $[Rh(CO)_2(MeCN)_2]BF_4$ (75 mg, 0.229 mmol) were treated with acetone (4 mL), and the solution, with some suspended material, was stirred for ∼2 h. Some insoluble material (mostly $[NMe_4]BF_4$) was filtered off and, prior to being discarded, washed with acetone (0.5 + 0.5 mL). The clear solution, with the collected washings, was cautiously layered with 2-propanol (24 mL). When the diffusion was completed (in about a week), black crystals of $[NMe_4]_2[Co_{10}Rh_2N_2(CO)_{24}]\cdot 2(Me_2CO)$ were separated from the mother liquor, thoroughly washed with 2-propanol, and briefly vacuum dried to avoid loss of the clathrated acetone. Yield: 130 mg, 65%. Anal. Found (calcd) (on freshly isolated samples, %) for $C_{38}H_{36}Co_{10}N_4O_{26}Rh_2$: C, 25.43 (25.94); H, 2.09 (2.06); N, 2.83 (3.18). No solid-state structure is available for this salt, but elemental analysis and IR are in agreement with the presence of 2 molecules of clathrated acetone, easily lost by evaporation.

2.b. Synthesis of $[Co_{10}Rh_2N_2(CO)_{24}]^{2-}$ (2) as $[NMe_4]^+$ or $[NEt_4]^+$ Salt through Cation Metathesis. A solution of $Cs_4[Co_{10}N_2(CO)_{19}]$ (120 mg, 0.0714 mmol) in acetone (3 mL) was treated at room temperature with $[Rh(CO)_2(MeCN)_2]BF_4$ (46.6 mg; 0.142 mmol). After it was stirred for 20 min, the solution was filtered to eliminate some insoluble material (mostly $CsBF_4$). The filtered solution was treated with a solution of $[NMe_4]Cl$ (1.2 g) in a mixture of 2-propanol (20 mL) and MeOH (2 mL) to induce precipitation by metathesis. The precipitate was filtered, washed with 2-propanol (3 × 1 mL), and vacuum dried. Extraction with acetone (3 mL) yielded a solution that was carefully layered with 2-propanol (10 mL). When the diffusion was completed (in about a week), the black crystals of the product were separated from the mother liquor, thoroughly washed with 2-propanol, and briefly vacuum dried. Yield: 32 mg, 27%. The IR spectrum in MeCN closely matched the reference spectrum in Table 4. The tetraethylammonium salt was obtained similarly after metathesis with $[NEt_4]Cl$, and crystals of $[NEt_4]_2[Co_{10}Rh_2N_2(CO)_{24}]$ proved suitable for the reported X-ray structure. Other ammonium or phosphonium salts can be obtained in a similar manner.

3. Synthesis of $[Co_{11}RhN_2(CO)_{24}]^{2-}$ (3) as $[NMe_4]^+$ Salt. $[NMe_4]_3[Co_{11}N_2(CO)_{21}]$ (56.7 mg, 0.0381 mmol) and $[Rh(CO)_2(MeCN)_2]BF_4$ (12.5 mg, 0.0381 mmol) were treated with acetone (1 mL) and stirred for ∼1 h at room temperature. After an IR check (see Table 4), the solution was carefully layered with 2-propanol (6 mL). When the diffusion was completed, nice black crystals of the product were separated from the mother liquor, washed thoroughly with 2-propanol (3 × 1 mL), and briefly vacuum dried to avoid loss of the clathrated acetone. Yield: 36 mg, 55%. Anal. Found (calcd) (on freshly isolated samples, %) for $C_{38}H_{36}Co_{11}N_4O_{26}Rh$: C, 26.62 (26.60); H, 2.04 (2.12); N, 3.11 (3.27). Elemental analysis and IR are in agreement with the presence of 2 molecules of clathrated acetone, rapidly lost by evaporation. The material maintains its solubility and spectroscopical purity (according to IR, see Table 4).

4.a. X-ray Data Collections for $[NMe_4]_3[Co_{10}RhN_2(CO)_{21}]\cdot[Me_2CO]$ and $[NMe_4]_2[Co_{11}RhN_2(CO)_{24}]\cdot[Me_2CO]_2$. Two crystals of dimensions 0.10 × 0.10 × 0.20 mm and 0.10 × 0.20 × 0.40 mm, respectively, were mounted on the tip of a thin glass fiber for X-ray examination and data collection. Data were collected at room temperature on a CAD4 diffractometer with graphite-monochromated Mo Kα radiation (λ = 0.71073 Å). Unit cell parameters were obtained by least-squares refinement of the angular settings of 25 intense reflections having $8 < \theta < 12°$. Crystal data and intensity collection parameters are given in Table 5. Intensity data were collected in the ω scan mode with $3 < \theta < 25$. Three standard reflections were monitored every hour and showed a gradual decrease of the scattering power of the crystals, which was evaluated as about 7 and 16% for $[NMe_4]_3[Co_{10}RhN_2(CO)_{21}]\cdot[Me_2CO]$ and $[NMe_4]_2[Co_{11}RhN_2(CO)_{24}]\cdot[Me_2CO]_2$, respectively, at the end of the data collection. The full data set was corrected for Lorentz, polarization, decay, and absorption effects. An empirical absorption correction was applied according to the method developed by North et al.[37] based on Ψ scans [Ψ = 0−360°, every 10°] of three reflections having χ values near 90°.

4.b. X-ray Data Collection for $[NEt_4]_2[Co_{10}Rh_2N_2(CO)_{24}]$. A crystal of dimensions 0.18 × 0.20 × 0.30 mm was mounted on the tip of a thin glass fiber for X-ray examination and data collection at room temperature on a Siemens SMART CCD area-detector diffractometer. Crystal data are presented in Table 5. Graphite-monochromatized Mo Kα (λ = 0.71073 Å) radiation was used with the generator working at 45 kV and 40 mA. Orientation matrices were initially obtained from least-squares refinement on ∼300 reflections measured in three different ω regions within the range of $0 < \theta < 23°$; cell parameters were optimized on the position, determined after integration, of ∼8000 reflections. The intensity data were collected within the limits $0 < 2\theta < 59°$ in the full sphere (ω scan method), with sample−detector distances fixed at 5.0 and 4.0 cm, respectively; 2400 frames (30 s per frame, $\Delta\omega = 0.3°$) were collected, and an empirical absorption correction was applied (SADABS[38]).

(37) North, A. C.; Phillips, D. C.; Scott Mathews, F. *Acta Crystallogr.* **1968**, *A24*, 351−359.
(38) Sheldrick, G. M. *SADABS*; University of Göttingen: Göttingen, Germany, 1996.

Table 5. Selected Crystallographic Parameters for $[NMe_4]_3[Co_{10}Rh(N)_2(CO)_{21}]\cdot[Me_2CO]$, $[NEt_4]_2[Co_{10}Rh_2(N)_2(CO)_{24}]$, and $[NMe_4]_2[Co_{11}Rh(N)_2(CO)_{24}]\cdot[Me_2CO]_2$

identification code	mart29	fu34	mart28
empirical formula	$C_{36}H_{42}Co_{10}N_5O_{22}Rh$	$C_{40}H_{40}Co_{10}N_4O_{24}Rh_2$	$C_{38}H_{36}Co_{11}N_4O_{26}Rh$
fw	1588.96	1755.88	1703.75
temp (K)	293(2)	293(2)	293(2)
wavelength (Å)	0.71073	0.71073	0.71073
cryst syst, space group	monoclinic, *P*21/*n*	monoclinic, *P*21/*c*	monoclinic, *C*2/*c*
a (Å)	17.223(4)	12.020(5)	23.608(5)
b (Å)	14.600(2)	18.370(5)	11.054(5)
c (Å)	22.326(6)	12.840(5)	22.550(5)
β (deg)	102.22(2)	108.500(5).	109.740(5)
vol (Å^3)	5487(2)	2688.7(17)	5539(3)
Z, density$_{calcd}$ (Mg/m^3)	4, 1.924	2, 2.169	4, 2.043
abs coeff (mm^{-1})	3.306	3.676	3.573
F(000)	3136	3440	3320
cryst size (mm)	0.10 × 0.10 × 0.20	0.18 × 0.20 × 0.30	0.10 × 0.20 × 0.40
θ range (deg)	3.04−25.02	1.79−34.43	3.02−24.98
limiting indices	$-20 \le h \le 20$	$-18 \le h \le 18$	$-28 \le h \le 26$
	$0 \le k \le 17$	$-28 \le k \le 29$	$0 \le k \le 13$
	$0 \le l \le 26$	$-20 \le l \le 20$	$0 \le l \le 26$
reflns collected/unique	9644/9644	39 676/10 827	4486/4486
	[*R*(int) = 0.0000]	[*R*(int) = 0.0463]	[*R*(int) = 0.0000]
decay	16%	none	7%
completeness, (θ)	99.6% (25.0)	95.5% (34.4)	92.0% (25.0)
abs correction	ψ-scan	SADABS	ψ-scan
max. and min. trans	0.9998 and 0.7031	1.000 and 0.8261	0.9999 and 0.6686
refinement method	full-matrix	full-matrix	full-matrix
	least-squares on F^2	least-squares on F^2	least-squares on F^2
data/restraints/params	9644/93/644	10 827/1/368	4486/19/359
GOF on F^2	0.959	0.981	1.048
final R indices	R1 = 0.0485	R1 = 0.0415	R1 = 0.0249
[$I > 2\sigma(I)$]	wR2 = 0.1218	wR2 = 0.0866	wR2 = 0.0700
R indices (all data)	R1 = 0.1803	R1 = 0.0697	R1 = 0.0363
	wR2 = 0.1628	wR2 = 0.0969	wR2 = 0.0730
largest diff. peak and hole (e Å^{-3})	1.002 and −0.750	1.262 and −0.552	0.612 and −0.478

4.c. X-ray Crystal Structure Determination of $[NMe_4]_3[Co_{10}RhN_2(CO)_{21}]\cdot[Me_2CO]$, $[NEt_4]_2[Co_{10}Rh_2N_2(CO)_{24}]$, and $[NMe_4]_2[Co_{11}RhN_2(CO)_{24}]\cdot[Me_2CO]_2$. The structures were solved by direct methods (SIR97[39]) and refined with full-matrix least-squares (SHELX97[40]) on the basis of 9644, 10 827, and 4486 independent reflections, respectively; anisotropic temperature factors were assigned to all non-hydrogen atoms. Hydrogen atoms were assumed to be riding on their carbon atoms. Ammonium cations were found to be crystal-disordered about one pseudo-threefold axis, and therefore, two sets of carbon atoms were modeled isotropically without their H atoms.

The crystals of $[NMe_4]_2[Co_{11}Rh(N)_2(CO)_{24}]\cdot[Me_2CO]_2$ were determined to consist of a solid solution of the two $[Co_{11}Rh(N)_2(CO)_{24}]^{2-}$ and $[Co_{10}Rh_2(N)_2(CO)_{24}]^{2-}$ anions in a 0.57:0.43 ratio. This substitutional disorder is not unreasonable given their "shape" similarity.

Acknowledgment. A. Fumagalli, A. Sironi, and P. Zanello gratefully acknowledge the financial support of their respective universities.

Supporting Information Available: X-ray crystallographic files in CIF format for **1**, **2**, and **3**, Figure 1S showing the EPR spectra of the electrogenerated $[Co_{10}Rh_2(N)_2(CO)_{24}]^{3-}$; anion $[\mathbf{2}]^-$ and $[Co_{10}Rh_2(N)_2(CO)_{24}]^{2-}$; (**2**) in CH_3CN solution at $T = 100$ K; Figure S2 showing an example of a check made by IR spectral subtraction evidencing an impurity in a sample of $[NMe_4]_2[Co_{10}Rh_2(N)_2(CO)_{24}]$ (**2**). This material is available free of charge via the Internet at http://pubs.acs.org.

IC0608288

(39) Altomare, A.; Burla, M. C.; Camalli, M.; Cascarano, G. L.; Giacovazzo, C.; Guagliardi, A.; Moliterni, A. G. G.; Polidori, G.; Spagna, R. *J. Appl. Cryst.* **1999**, *32*, 115−119.

(40) Sheldrick, G. M. *Programs for Crystal Structure Analysis*, release 97-2; Institüt für Anorganische Chemie der Universität: Göttingen, Germany, 1998.